This is the Pre-Published Version.
S. Lin, S. Wang, X. Huang (2022) *Modeling Smoldering Ignition by an Irradiation Spot*, **Fire Safety Journal**, 103708.
https://doi.org/10.1016/j.firesaf.2022.103708

Modeling Smoldering Ignition by an Irradiation Spot

Shaorun Lin[a,b], Siyan Wang[a,c], Xinyan Huang[a,*]

[a] *Research Centre for Fire Safety Engineering, The Hong Kong Polytechnic University, Hong Kong*

[b] *The Hong Kong Polytechnic University Shenzhen Research Institute, Shenzhen, China*

[c] *Department of Mechanical Engineering, University of California, Berkeley, CA, USA*

*Corresponding to xy.huang@polyu.edu.hk (X.H)

Abstract

Irradiation spots, such as lasers, lightning strikes, and concentrated sunlight, are common ignition sources in building and wildland fires, where smoldering is generally first ignited and then transitions to flaming. In this work, a physics-based 2-D computational model that integrates heat-and-mass transfer and heterogeneous chemistry is built to investigate the smoldering ignition of typical solid fuels using irradiation spots. Simulation results predict that, given the size of the irradiation spot, the ignition time decreases as the radiant heat flux increases. However, as the diameter of the irradiation spot decreases, the modeled minimum heat flux of smoldering ignition increases significantly, agreeing well with experiments and theoretical analysis. When the irradiation spot is smaller than 20 mm, assumptions of constant ignition temperature and fuel-burning flux become invalid, and the commonly-used physical dimensions of thermally thin/thick fuels are not applicable due to the significant radial conductive heat loss in the lateral direction. Further analyses show that the minimum irradiation of smoldering ignition increases as the fuel thickness increases, but it is insensitive to the fuel moisture content. This is the first time that a sophisticated 2-D model has been used to predict the smoldering ignition using irradiation spots, which deepens the understanding of the ignition by a remote heating source and large irradiation.

Keywords*: High irradiation; Spotting fire; Ignition limit; Smoldering fire; Numerical simulation.*

1. Introduction

Understanding the ignition of combustible materials is significant to fire safety assessment [1], which is an essential process to enrich firefighting strategies and provide a scientific foundation for performance-based fire safety design. In real fire scenarios, spotting is a common ignition mechanism in structures and wildlands [2–4], such as the lofted firebrands [3,5], hot (metal) particles [6–10], dripping plastic fuels [11,12], laser or nuclear irradiation [13], lightning strikes [14], and concentrated (solar) irradiation spots [13,15]. Previous studies on spotting ignition by lofted firebrands have established many insightful understandings which improve fire safety in the wildland-urban interface.

Nomenclature

Symbols		*Greeks*	
A	pre-exponential factor (1/s) or area (m^2)	α	absorptivity (-)
c	specific heat capacity (J/kg-K)	γ	radiative conductivity coefficient (m)
D	diffusivity (m^2/s)/diameter of irradiation spot (m)	δ	thickness (m)
D_{eff}	effective diffusivity (m^2/s)	ε	emissivity (-)
E	activation energy (kJ/mol)	κ	permeability (m^2)
$\bar{h}$	specific enthalpy (J/kg)	ρ	density (kg/m^3)
h	convective coefficient (W/m^2-K)	ν	viscosity (Pa · s)/stoichiometry (-)
h_m	mass-transfer coefficient (kg/m^2-s)	ψ	porosity (-)
H	height (m)	$\dot{\omega}'''$	volumetric reaction rate (kg/m^3-s)
ΔH	heat of combustion (MJ/kg)		
k	thermal conductivity (W/m-K)	*Subscripts*	
m	mass (kg)	∞	ambient
$\dot{m}''$	mass flux (kg/m^2-s)	*cond*	conduction
M	molar mass (kg/mol)	*d*	destruction
MC	moisture content (%)	*dr*	drying
n	reaction order (-)	*f*	formation
P	pressure (Pa)	*g*	gas
$\dot{q}''$	heat flux (kW/m^2)	*i*	condensed species number
R	thermal resistance (m^2-K/W)	*ig*	ignition
S	surface area (m^2)	*ir*	irradiation
t	time (s)	*j*	gaseous species number
T	temperature (°C or K)	*k*	reaction number
X	volume fraction (-)	*o/ox*	oxidation
Y	mass fraction (-)	*p*	pyrolysis
Δz	cell size (m)	*s*	solid
		sm	smoldering

For example, Manzello et al. [3] provided a comprehensive review of the role of firebrand mechanisms on large outdoor fire spread, including the experiments, models, and simulations related to firebrand generation, lofting, burning, transport, deposition, and ignition of materials. Comparatively, our understandings of the ignition by small spots of high irradiation, such as laser and concentrated sunlight, are still quite limited. In July 2018, the Fisher 231 fire that burned roughly 80 acres near Reardan, Washington, was initiated by sunlight irradiation spots concentrated by shards of broken glass [16]. However, the underlying mechanism of such ignition events has not been well studied yet, particularly for smoldering ignition.

Smoldering is a slow, low-temperature, and flameless combustion phenomenon [17]. Smoldering is sustained by the heat evolved when oxygen molecules directly attack the hot surface of condensed-phase reactive porous media [18,19]. In general, smoldering is easier to be triggered than flaming in terms of the minimum ignition irradiation [20]. Therefore, smoldering provides a shortcut to flaming fire through the smoldering-to-flaming transition [21,22], making it the primary cause and driving phenomenon of devastating fire events [23]. However, previous research mainly focused on the smoldering ignition where the entire fuel surface is uniformly heated (e.g., cone-calorimeter tests) [20,24–26], while the ignition event caused by irradiation spots has not been well studied yet, presenting a knowledge gap.

The most common spotting ignition phenomenon is caused by firebrands, which is a complex process including the transfer of both a heat source and fuel (firebrands can act as fuel and heating source simultaneously) [4,9]. Comparatively, the smoldering ignition by an irradiation spot only involves an energy transfer process. Therefore, such an ignition event is more straightforward, providing significant references for more complex spotting ignition processes. So far, only limited experiments have been conducted for the flaming ignition by laser spots or light beams [27–30], while the smoldering ignition by tiny irradiation spots is rarely studied. In 1965, Martin [31] investigated the auto-flaming ignition of cellulosic materials using a 2.3-cm irradiation spot and found that the ignition temperature remained constant at 600-650 ^{o}C, regardless of the irradiation levels. These values are much higher than the auto-ignition threshold of uniform-heated cellulosic materials [32,33]. Similarly, Kashiwagi [28,29] applied a laser spot with a diameter of 2-3 cm and found that the minimum irradiant heat fluxes for flaming autoignition were 90 kW/m^2 for red oak and 160 kW/m^2 for PMMA respectively, which are also much higher than 25-50 kW/m^2 obtained under cone calorimeter. Grishin et al. [34] revealed that the required irradiant heat flux for flaming ignition of a porous forest fuel layer decreased from around 43 kW/m^2 to 20 kW/m^2 as the irradiation spot diameter increased from 8 mm to 27 mm. From the aforementioned studies, the ignition thresholds for flaming fires are not constant but vary with the heating areas.

Considering there are many similarities between flaming and smoldering fire behaviors [18], it is reasonable to expect that the ignition threshold of smoldering may also be sensitive to the heating area. Recently, we studied the smoldering ignition of tissue papers by concentrated solar irradiation spots and found that the minimum irradiation for smoldering ignition increased from 17.5 kW/m^2 to 205 kW/m^2, as the diameter of the irradiation spot decreased from 20 mm to 1.5 mm [13,35]. Over the past few decades, some sophisticated numerical studies on the flaming ignition by irradiation spots have also enriched our understanding of its ignition mechanism. For example, Nakamura and Kashiwagi [30] established a numerical model including heat and mass transport processes with global one-step chemical reactions in both gas and solid phases to investigate the ignition processes of a thin polymethyl methacrylate (PMMA) using a laser beam. They found that the formation of a hole through the thin sample can reduce the fuel supply rate but increase the air supply from the back side to the irradiated

side by the buoyancy-induced flow. However, to the best of the authors' knowledge, no computational model is available yet to reveal the smoldering ignition phenomenon initiated by irradiation spots.

Since the 2000s, many 1-D numerical simulations have been conducted to investigate the smoldering processes of different reactive porous media with different complexities [36–39]. However, the 1-D model can only investigate the heating and ignition under uniform irradiation. For spotting ignition, the multi-dimensional heat transfer in the solid is critical; thus 1-D model is not applicable. Recently, we successfully established a physics-based 2-D computational model to reproduce the quenching and near-limit propagation of smoldering [40], which laid a foundation for exploring the smoldering ignition by irradiation spots.

This work develops a comprehensive 2-D model for smoldering ignition of biomass fuel using irradiation spots based on open-source code Gpyro [41] and a previously developed 5-step smoldering kinetic scheme of typical biomass fuel [42–44]. The sample is heated by irradiation spots with different diameters. Simulations quantify the ignition time and minimum heat flux of smoldering ignition. Afterwards, the influences of the sample thickness and moisture content on spotting smoldering ignition processes are explored.

2. Computational model

2.1. Model establishment

Our previous experiments have studied the smoldering ignition of 2-mm thick tissue papers by a concentrated solar irradiation spot for the first time [13,35]. As the simulation of these experiments is the starting point of this work, a brief introduction to the experiments is given here.

The 2-mm (six layers) tissue paper used in the experiments was completely made of pure unbleached pulp (i.e., wood fiber); thus, it could be regarded as biomass fuel whose smoldering process could be explained by the 5-step kinetics applied here [42–44]. The influence of the gap between layers could be characterized by the fuel bulk density [13]. The sunlight was concentrated by a transparent glass sphere with a diameter of 150 mm. Optical simulations using *Tracepro* (a powerful and versatile design and analysis environment for illumination systems and non-imaging aspects of optical systems that can accurately and quickly predict spatial and angular light output distribution, uniformity, intensity, and spectral characteristics) and a radiometer were used to quantify the sizes of light spots and irradiation levels [13]. Solar irradiation spots with four heating diameters (D) of 20.0 mm, 9.0 mm, 5.5 mm, and 1.5 mm were tested to find the time of smoldering ignition under different irradiations up to 780 kW/m^2. For a larger irradiation spot, the critical irradiation of ignition is low.

Due to losses resulting from reflection, refraction, and spherical aberration, it is extremely difficult to find the exact position of the low irradiation level within the focus length, which could also result in a large uncertainty. Therefore, the cone calorimeter was applied here to provide a reference value with a larger heating diameter of 60 mm. In total, more than 600 tests were conducted outdoors on typical sunny days in summer, and the ignition boundaries were obtained based on statistical analysis. A

detailed description of the experiments could be found in [13,35]. Experiments showed that, with a fixed size of the irradiation spot, the smoldering ignition time decreased as the concentrated irradiation increased, analogous to the classical piloted flaming ignition theory. However, as the diameter of the irradiation spot decreased from 60 mm to 1.5 mm, the minimum irradiation for smoldering ignition gradually increased from 11 kW/m^2 to 205 kW/m^2.

As spotting ignition by irradiation spots is essentially a multi-dimensional process, herein, a 2-D numerical model is developed using Gpyro v0.8 [41], which is a generalized open-source code for reactive porous media such as peat, wood and coal [45–47]. Gpyro is capable of calculating the transient composition of species (both reactants and products) at different locations. By coupling the solver with separate transient conservation equations of gaseous and condensed-phase mass, species, and energy, the temperature and species distributions inside the reacting porous media can be well simulated. The schematic diagram of the computational domain is shown in Fig. 1, which has the same sample thickness (2 mm) and length (60 mm) as that in our previous experiments [13,35]. The irradiation spots with different diameters are applied to the middle of the upper surface. To save computational cost, the domain can be half of the actual sample owing to geometrical symmetry [40], as illustrated in Fig. 1.

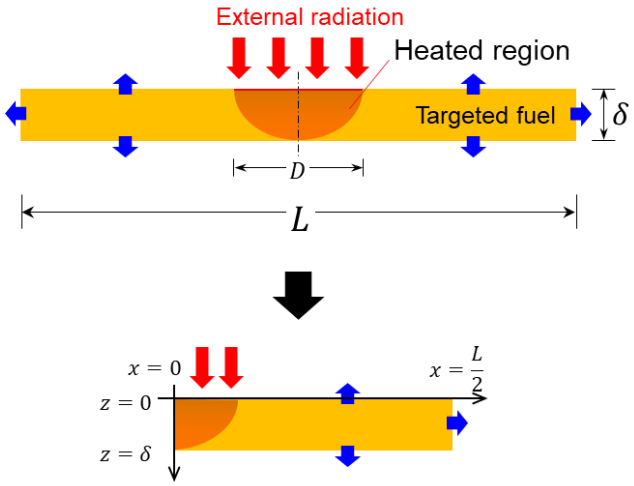

Fig. 1. Schematic diagram of the 2-D computational domain for smoldering ignition using irradiation spots, where red and blue arrows represent heating and cooling respectively.

Initially, the same diameters of irradiations as those in the experiments (1.5 mm, 5.5 mm, 9.0 mm, 20 mm and 60 mm) are applied in the computations to validate the accuracy of our model. Given the size (D) and intensity ($\dot{q}''_{ir}$) of the irradiation spot, the simulation is started with a prescribed heating duration. If smoldering is successfully initiated and subsequently self-sustains (based on 2-D temperature profiles (e.g., Fig. 2)), the heating duration is adjusted to find the limiting ignition time (t_{ig}) under given irradiation. Eventually, smoldering ignition will not be triggered with a smaller radiant heat flux under a long heating duration ($t_{ig} \to \infty$), defined as minimum heat flux for smoldering ignition ($\dot{q}''_{min}$). Note that the interval of adjustment is not constant, as the $\dot{q}''_{ir}$ or t_{ig} decreases, the intervals are

required to decrease as well but it is generally small than the 5% of the obtained value. Afterward, the sizes (up to 60 mm) and irradiation levels (up to 400 kW/m^2) of the spots, the thicknesses (from 2 mm to 15 mm) and the moisture contents (from 0% to 50 %) of the target fuels are varied to give a full picture of the limiting conditions of smoldering ignition using small irradiation spots. In total, more than 600 simulations were performed.

2.2. 2-D governing equations

The gravity and buoyancy effect inside the porous media of such a small fuel sample plays a negligible role, as found in our preliminary simulations [40,48]. Therefore, the model solves the 2-D transient conservation equations for condensed and gaseous phases in the absence of gravity, and thermal equilibrium is assumed between gas and condensed-phase species [41]. The governing conservation equations are provided here, including the conservation of mass (Eq. 1), species (Eq. 2) and energy (Eq. 3) in the condensed phase as well as the mass (Eq. 4), species (Eq. 5), and momentum (Darcy's law) (Eq. 6) in the gas phase. The subscripts *i*, *j*, and *k* represent the number of condensed-phase species, gas-phase species, and reactions, *d* and *f* refer to the destruction and formation of species, and *z* and *x* refer to vertical and horizontal directions, respectively. Gaseous diffusion coefficients are calculated from Chapman–Enskog theory, and the detailed model could be found in [49,50].

$$\frac{\partial \bar{\rho}}{\partial t} = -\dot{\omega}'''_{fg} \tag{1}$$

$$\frac{\partial (\bar{\rho} Y_i)}{\partial t} = \dot{\omega}'''_{fi} - \dot{\omega}'''_{di} \tag{2}$$

$$\frac{\partial (\bar{\rho}\bar{h})}{\partial t} = k\frac{\partial}{\partial x}\left(\frac{\partial T}{\partial x}\right) + k\frac{\partial}{\partial z}\left(\frac{\partial T}{\partial z}\right) + \dot{\omega}'''_{di}(-\Delta H_i) \tag{3}$$

$$\frac{\partial}{\partial t}(\rho_g \overline{\psi}) + \frac{\partial \dot{m}''_x}{\partial x} + \frac{\partial \dot{m}''_z}{\partial z} = \dot{\omega}'''_{fg} \tag{4}$$

$$\frac{\partial}{\partial t}(\rho_g \overline{\psi} Y_j) + \frac{\partial}{\partial x}(\dot{m}''_x Y_j) + \frac{\partial}{\partial z}(\dot{m}''_z Y_j) = -\frac{\partial}{\partial x}\left(\overline{\psi}\rho_g D_{eff}\frac{\partial Y_j}{\partial x}\right) - \frac{\partial}{\partial z}\left(\overline{\psi}\rho_g D_{eff}\frac{\partial Y_j}{\partial z}\right) + \sum \dot{\omega}'''_j \tag{5}$$

$$\dot{m}''_z = -\frac{\kappa}{\nu}\frac{\partial p}{\partial z} \quad \dot{m}''_x = -\frac{\kappa}{\nu}\frac{\partial p}{\partial x} \qquad \left(\rho_g = \frac{P\overline{M}}{RT}\right) \tag{6}$$

For the symmetrical plane ($x = 0$), adiabatic and impermeable boundary conditions are applied, as described in Eqs. (7) and (8). At the top free surface ($z = 0$), initially ($t \le t_h$), an irradiation ($\dot{q}''_{ir}$) with a heating diameter of $D/2$ is applied for a prescribed duration (t_h), and both convective ($h_{c,z=0} = 1.52(T_{ig} - T_\infty)^{1/3} \approx 10\ \mathrm{W/m^2 \cdot K}$) and radiative heat losses ($\varepsilon = 0.9$) are considered [37,51]. Afterwards ($t > t_h$), the irradiation spot is removed (Eq. 9). The mass transfer of gas species on the top free surface is calculated through Eq. (10). Based on the heat-mass transfer analogy, the mass transfer coefficient can be approximated as $h_{m,z=0} = h_{c,z=0}/C_g = 9.09\ \mathrm{g/m^2 \cdot s}$, where C_g is the specific heat capacity of gas species and is assumed to be constant at $1{,}100\ \mathrm{J/kg \cdot K}$ in the simulation [41].

At the right and bottom boundary ($z = \delta$ and $x = L/2$), similar to the top free surface, both convective ($h_{c,z=0} = 10\ \mathrm{W/m^2 \cdot K}$) and radiative heat losses are considered, and the same mass transfer of gas species as the top surface is applied on the bottom surface. The ambient pressure and temperature are assumed to be 1 atm and 300 K. The whole computational domain has the same initial gas composition as the ambient air ($Y_{O_2} = 0.232$ and $Y_{N_2} = 0.768$). The solution starts to converge at $\Delta z = \Delta x = 0.1$ mm and $\Delta t = 0.01$ s. Further reducing the cell size and time step by a factor of two gives no significantly different results, so the calculations are sufficiently resolved.

$$k\frac{\partial T}{\partial x}\bigg|_{x=0} = 0 \tag{7}$$

$$\bar{\psi}\rho_g D_{eff}\frac{\partial Y_j}{\partial x}\bigg|_{x=0} = 0 \tag{8}$$

$$-k\frac{\partial T}{\partial x}\bigg|_{z=0,0\le x\le \frac{D}{2}} = \begin{cases} \dot{q}''_{ir} - h_{c,z=0}(T|_{z=0} - T_\infty) - \varepsilon\sigma(T^4|_{z=0} - T_\infty^4)\ (t \le t_h) \\ -h_{c,z=0}(T|_{z=0} - T_\infty) - \varepsilon\sigma(T^4|_{z=0} - T_\infty^4)\ (t > t_h) \end{cases} \tag{9}$$

$$-\bar{\psi}\rho_g D_{eff}\frac{\partial Y_j}{\partial x}\bigg|_{z=0} = -h_{m,z=0}\left(Y_j|_{z=0} - Y_j^\infty\right) \tag{10}$$

2.3. Smoldering kinetics

Because the tissue sample used here was completely made of pure unbleached pulp (i.e., wood fiber), a previously developed 5-step kinetic scheme of typical biomass, which has been used to simulate the smoldering of peat [42], wood [43], fiberboard [44], and other reactive porous media with similar components, has been applied here. As moisture usually exists in biomass fuels, the low-temperature drying process occurs first which can be expressed as

$$\text{Water} \rightarrow \text{Water vapor} \qquad [\text{dr}] \quad (11)$$

In general, natural biomass has three major components with different pyrolysis temperatures: hemicellulose (~250 ℃), cellulose (~300 ℃), and lignin (~350 ℃) [52]. Their pyrolysis processes can be expressed by a 3-step pyrolysis kinetic scheme as

$$\text{Hemicellulose} \rightarrow \text{Char} + \text{Pyrolyzates} \qquad [\text{hp}] \quad (12)$$

$$\text{Cellulose} \rightarrow \text{Char} + \text{Pyrolyzates} \qquad [\text{cp}] \quad (13)$$

$$\text{Lignin} \rightarrow \text{Char} + \text{Pyrolyzates} \qquad [\text{lp}] \quad (14)$$

For modeling any smoldering combustion, char oxidation (Eq. 15) has to be included in the model.

$$\text{Char} + \text{O}_2 \rightarrow \text{Ash} + \text{gas} \qquad [\text{co}] \quad (15)$$

The normalized reaction rate of reaction (k) and reaction (A) can be expressed by Arrhenius law

$$\dot{\omega}_k^* = Z_k \exp\left(-\frac{E_k}{RT}\right) f(m_A^*) g\left(Y_{O_2}\right) \tag{16}$$

where Z_k is the pre-exponential factor, and E_k is the activation energy. The function for mass action of reactant A is

$$f(m_A^*) = (m_A^*)^{n_k} = \left(\frac{m_A}{m_{sA,0}}\right)^{n_k} \tag{17}$$

where $m_{sA,0}$ is the original mass of the species A, and n_k is the reaction order. The oxidation model considers oxidative pyrolysis as

$$g\left(Y_{O_2}\right) = \begin{cases} 1 & (n_{k,O_2} = 0) \\ \left(1 + Y_{O_2}\right)^{n_{k,O_2}} - 1 & (n_{k,O_2} > 1) \end{cases} \tag{18}$$

where n_{k,O_2} is the order of oxidation. The kinetic parameters for the smoldering of biomass are obtained by optimizing the TG data in both inert and oxidative atmospheres using the Kissinger-Genetic Algorithm method (see detailed description in [44]) and are listed in Table 1. Different from homogenous gas-phase flame reactions, all smoldering reactions are heterogenous that occur on the interface between gas and solid, and the same kinetics of smoldering can be used to simulate ignition, propagation and extinction [40,46,53]. The averaged properties in each cell are calculated using the appropriate mass fraction or volume fraction. For simplification, all gaseous species are assumed to have unit Schmidt number, same diffusivity and specific heat [40,54].

The detailed species thermophysical properties can be found in [43] and Table 2. Note that the establishment of the model involves several assumptions. For example, the input of the physical properties of fuels and their sensitivities to temperature are simplified as constant, and the model does not include the microscopic structure and inhomogeneity of fuel particles. However, our previous work has demonstrated our model's capability to simulate the ignition, propagation and extinction of smoldering combustion with satisfactory accuracy [40].

Table 1 Chemical kinetic parameters and yields of 5-step reaction for biomass, where the reaction expression is $A_k + \nu_{O_2,k} O_2 \rightarrow \nu_{B,k} B_k + \nu_{g,k}$gas, and $\Delta H > 0$ is endothermic.

Parameter	*dr*	*hp*	*cp*	*lp*	*co*
$\lg Z_k$ (lg (s^{-1}))	8.12	8.2	11.4	21.4	12.9
E_k (kJ/mol)	67.8	106	154	229	184
n_k (-)	3	1.49	0.95	8.7	1.27
n_{k,O_2} (-)	0	0	0	0	1
$\nu_{B,k}$ (kg/kg)	0	0.24	0.27	0.40	0.06
ΔH_k (MJ/kg)	2.26	0.2	0.2	0.2	-20
$\nu_{O_2,k}$ (kg/kg)	0	0.5	0.5	0.5	1.5

Table 2 Physical parameters of condensed species [43].

Species	Y_0 (-)	ρ (kg/m^3)	k (W/m-K)	c (J/kg-K)
Water	0 (dry)	1000	0.60	4200
Hemicellulose	0.209	150	0.05	1500
Cellulose	0.529	150	0.05	1500
Lignin	0.262	150	0.05	1500
Char	0	100	0.03	3000
Ash	0	15	0.01	3000

3. Modeling results and analysis

3.1. Base cases

To better understand the transient smoldering ignition process, the 2-D profiles of temperature and volumetric reaction rate of two base cases are shown simultaneously here (Fig. 2), where the left and right sides of the symmetric plane represent the 2D profiles of temperature and volumetric reaction rate, respectively. With a heating diameter of 5 mm, right after heating for 100 s, a hot region (>500 °C) with intense heat emitted emerges at the irradiated region, as shown in Fig. 2(a) and Video S1. Afterwards, the hot smoldering zone gradually spreads outwards at a near-constant rate of about 0.15 cm/s until reaching the end and burnout.

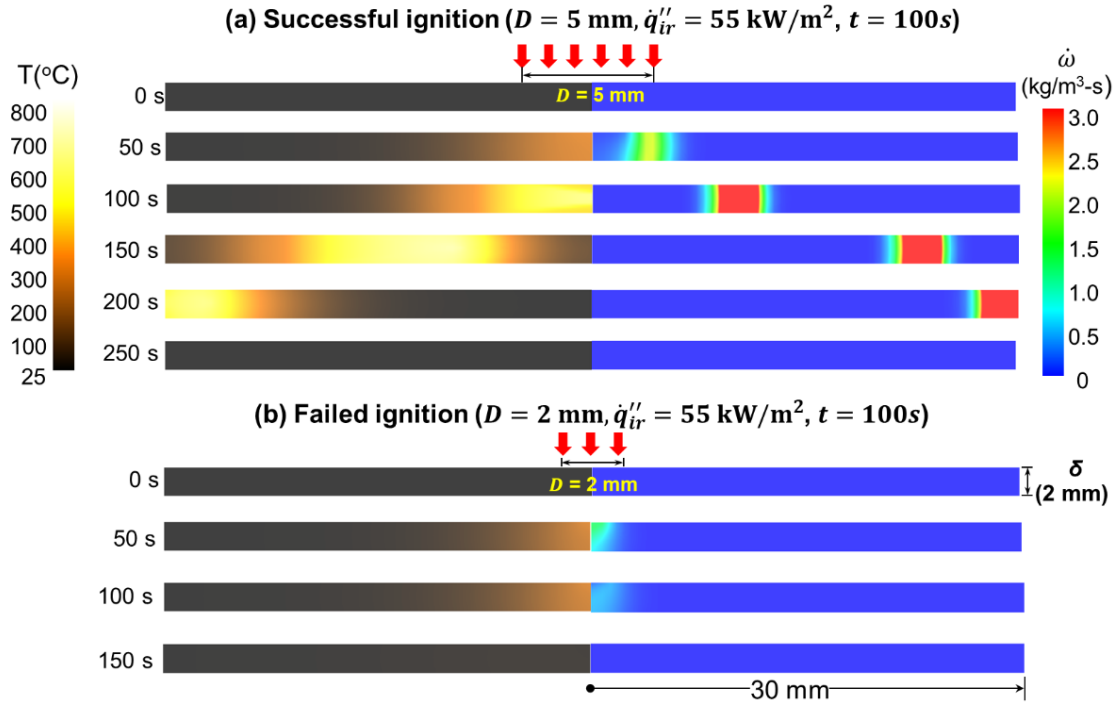

Fig. 2. Profiles of temperature and volumetric reaction rate of (a) ignition with D = 5 mm, and (b) failed ignition with D = 2 mm, where irradiation is $\dot{q}''_{ir} = 55$ kW/m^2 for 100 s.

By keeping the same irradiation of 55 kW/m^2 while decreasing the heating diameter to 2 mm, the heating process is shown in Fig. 2(b) and Video S2. After being heated for 100 s, the sample temperature reaches about 300 ^{o}C. Then, the temperature of the hot spot quickly decreases to the ambient temperature. With the same irradiation spot, increasing the heating duration to 1000 s, ignition is still not successful. In other words, the minimum irradiation of smoldering ignition by the 2-mm spot is larger than 55 kW/m^2.

Fig. 3 further compares the simulated mass loss flux in the irradiated zone of these two base cases, where the mass flux was calculated within the irradiated area. For the ignited case (D = 5 mm), once the irradiation is applied, the mass-loss flux quickly increases above 1 g/m^2-s within 10 s. By continuing the heating, a further increase is observed at about 60 s, indicating the formation of a stable smoldering front. The fuel-burning flux peaks at 170 s when the smoldering front reaches the edge (see Fig. 2a). Afterwards, it gradually decreases to zero as the entire fuel burns out. On the other hand, for the failed ignition case, during the irradiative heating for 100 s, the maximum burning flux is lower than 1 g/m^2-s. Once the irradiation stops, the burning flux rapidly drops to zero, the same as the temperature and volumetric reaction rate in Fig. 2(b), so that a robust smoldering front is not formed. More discussions on the critical mass flux could be found in Section. 3.3.

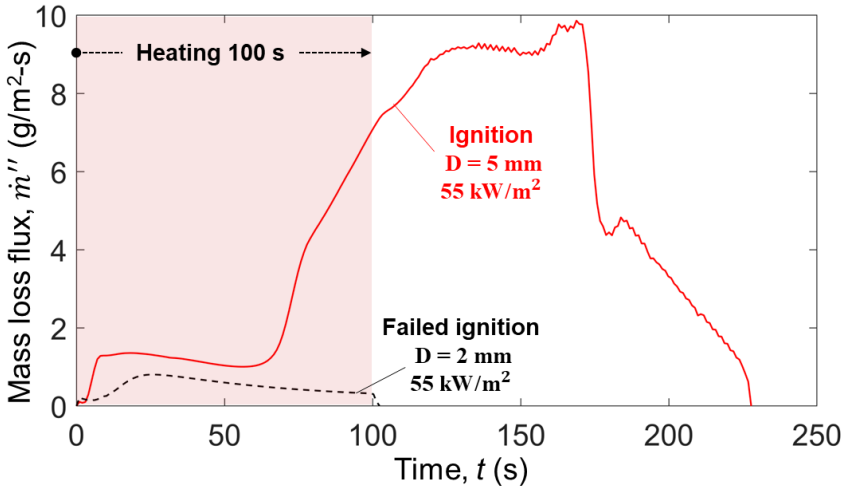

Fig. 3. Predicted mass loss flux of successful (red solid line) and failed (black dashed line) smoldering ignition.

3.2. Model validation by experiments

Fig. 4(a) summarizes the modeled ignition time (solid lines) and compares it with the experimental data (markers, uncertainty shown by shadowed area) [35]. Considering the complex nature of the smoldering process, a good agreement can be observed between predictions and experiments. Also, the effect of irradiation level ($\dot{q}''_{ir}$) on the ignition time is well predicted by the model; that is, the ignition time decreases as the irradiation level increases. For example, given an irradiation spot of 5 mm, as the radiant heat flux increases from 60 kW/m^2 to 150 kW/m^2, the predicted ignition time decreases from 85 s to 8 s. On the other hand, under a fixed irradiation level, the ignition time decreases as the heating

diameter increases. For example, given an irradiation level of 300 kW/m^2, as the diameter of the irradiation spot increases decreases from 20.0 mm to 1.5 mm, the ignition increases from less than 1 s to around 25 s.

By considering the absorptivity of the fuel, the size effect of irradiated area (which contributes to the conductive heat loss) and ambient heat loss, all data on ignition delay time can be fitted into an empirical correlation based on the modified thermally-thin theory ($t_{ig} = \left(\rho\delta c_p(T_{sm} - T_\infty)\right)/\dot{q}''_{ir}$) [23]

$$t_{ig} = \frac{\rho\delta\left(\mathrm{MC}\cdot\Delta H_{ev} + c_p(T_{sm} - T_\infty) + \Delta H_{py}\right)}{\left(\alpha\dot{q}''_{ir} - \frac{C}{D} - 2\dot{q}''_\infty\right)} \tag{18}$$

where the $\alpha = 0.7$ is the absorptivity [55], $C = 300$ W/m is the size coefficient obtained from the fitting, $\dot{q}''_\infty = \varepsilon\sigma(T_{sm}^4 - T_\infty^4) + h(T_{sm} - T_\infty) = 5.5$ kW/m^2 is the heat loss from the top and bottom fuel surfaces [23], c_p is the specific heat, ΔH_{ev} is the heat of water evaporation, ΔH_{py} is the heat of pyrolysis, and T_{sm} is the smoldering ignition temperature [18] (see Section 3.3). A satisfactory degree of fit could be achieved with a $R^2 > 0.95$.

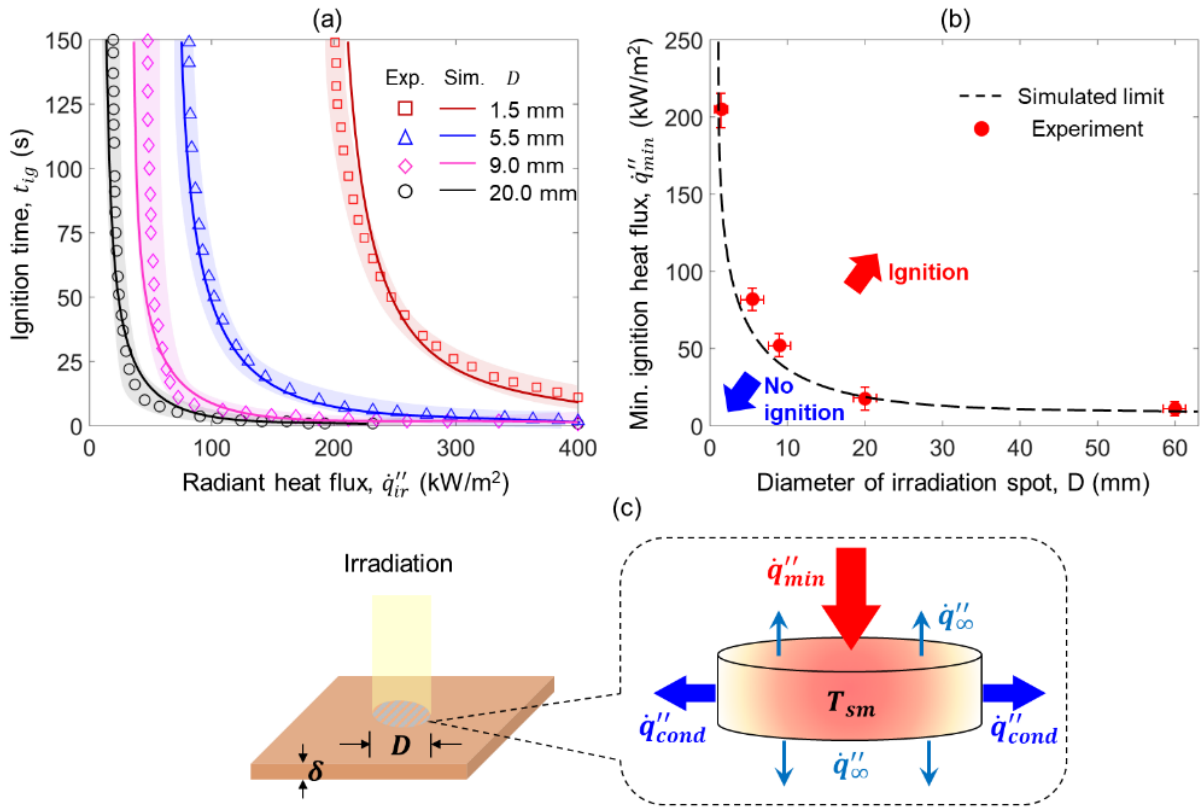

Fig. 4. (a) Comparison between the experimental and modelled ignition time under different irradiation spots, (b) predicted minimum heat flux of smoldering ignition vs. test data [13,35], and (c) diagram of smoldering spotting ignition.

Fig. 4(b) further summarizes the predicted minimum heat fluxes of smoldering ignition ($\dot{q}''_{min}$) for different irradiation spots and compares them with the experimental data [35]. For example, as the

diameter of the irradiation spot increases from 2 mm to 10 mm, the predicted minimum heat flux for smoldering ignition decreases from 85 kW/m^2 to 43 kW/m^2. In general, simulations show an excellent agreement with experimental measurements with a relative error of less than 10%, so the numerical model is further validated.

To better explain the influence of internal radial conductive heat loss on the minimum radiant heat flux of smoldering ignition, a simplified heat transfer analysis based on energy conservation is proposed for a thin sample heated by an irradiation spot. As shown in Fig. 4(c), at the ignition threshold, the minimum heat flux ($\dot{q}''_{min}$) should just balance the heat loss from the top and bottom fuel surfaces ($\dot{q}''_{\infty}$) and radial conductive heat loss to the virgin fuel ($\dot{q}''_{cond}$) as

$$\dot{q}''_{min}\left(\frac{\pi D^2}{4}\right) = \dot{q}''_{\infty}\left(\frac{\pi D^2}{4}\right) \times 2 + \dot{q}''_{cond}(\pi D\delta) \tag{19a}$$

which can be further expressed and simplified as

$$\dot{q}''_{min} = 2\dot{q}''_{\infty} + \frac{4\delta \dot{q}''_{cond}}{D} \tag{19b}$$

From Eq. (19b), the minimum heat flux of smoldering ignition ($\dot{q}''_{min}$) increases as the diameter of the irradiation spot (D) decreases, explaining the trend in Fig. 4(b). Moreover, as the diameter of the irradiation spot approaches infinity, the conductive loss can be neglected and the problem approaches a 1-D scenario.

3.3. Spotting ignition criteria

The ignition temperature and the fuel-burning flux are often used to quantify the limiting conditions for ignition. Under uniform irradiation, their values are almost constant near the moment of ignition [23]. Fig. 5 summarizes (a) the modeled surface ignition temperature (T_{ig}) and (b) the minimum fuel mass flux ($\dot{m}''_{min}$) within the irradiated spot for the smoldering ignition vs. different spot diameters. When the spot diameter is small (D < 20 mm), both the predicted ignition temperature and minimum mass flux dramatically increase as the diameter of the irradiation spot decreases.

For example, as the spot diameter decreases from 20 mm to 5 mm, the ignition temperature and minimum mass flux within the irradiated area increase from around 325 ^{o}C and 2 g/m^2-s to 400 ^{o}C and 13 g/m^2-s, respectively. It may be because the small heated zone on the sample needs to further raise the nearby area above the smoldering temperature by the solid-phase conduction to form a robust smoldering front. Thus, the fuel temperature within the spot increases rapidly to raise the local burning flux. Therefore, the definition of constant critical ignition temperature ($T_{ig,crt}$) and minimum mass flux ($\dot{m}''_{min}$) is no longer appropriate to characterize smoldering spotting ignition when the targeted fuel was only heated by tiny irradiation spots.

Comparatively, as the heating diameter increases, eventually, for large spot diameter (when D is larger than 20 mm), a constant critical burning flux on the order of 1 g/m^2-s and a critical surface

temperature of around 300 ºC are required to trigger smoldering combustion, as shown in Fig. 5. Such values are consistent with the literature experiments under uniform irradiations [20,56]. At this moment, the ignition could be simplified as a 1-D process where the internal conductive heat loss becomes negligible.

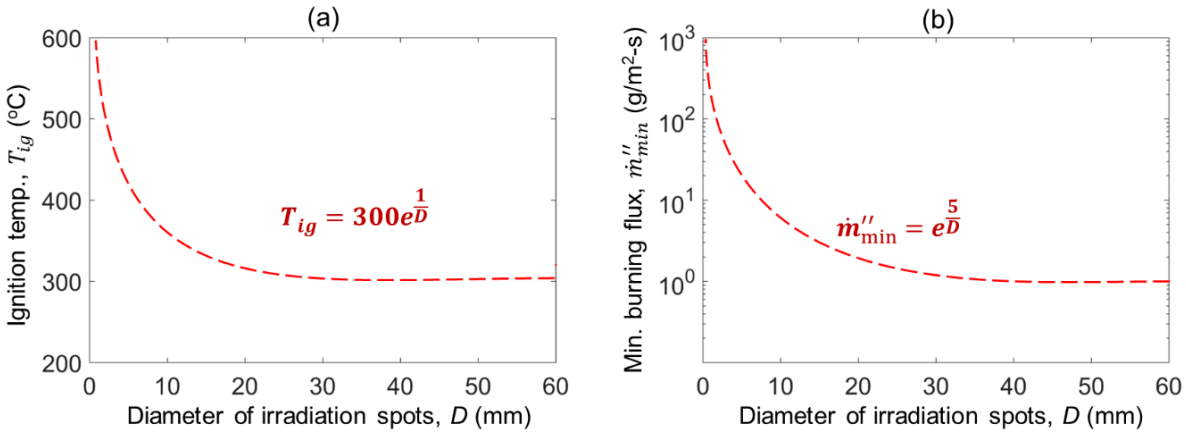

Fig. 5. (a) Ignition temperature and (b) burning flux for smoldering ignition in the spotted region, where the fuel thickness is δ = 2 mm, and the unit of D in correlations is mm.

3.4. Effect of fuel thickness

During the experiments, the thickness (δ = 2 mm) of dry tissue paper is fixed, so its influences on spotting smoldering ignition have not been revealed. By varying the sample thickness (δ) from 1 mm to 15 mm in the numerical model, the thickness effect on the smoldering spotting ignition limit is investigated. Fig. 6 shows the ignition time vs. irradiation for different fuel thicknesses (δ) and spot diameters (D), where the modeled ignition time also decreases as the radiant heat flux increases. On the other hand, the ignition time is found to increase with the sample thickness, showing the characteristics of a thermally-thin fuel (where the ignition time shows a dependence on the thickness of the sample). For example, given a spot diameter of 5 mm and irradiation of 150 kW/m^2, the ignition time increases by more than 10 times from 8 s to 90 s, as the sample thickness increases from 2 mm to 10 mm.

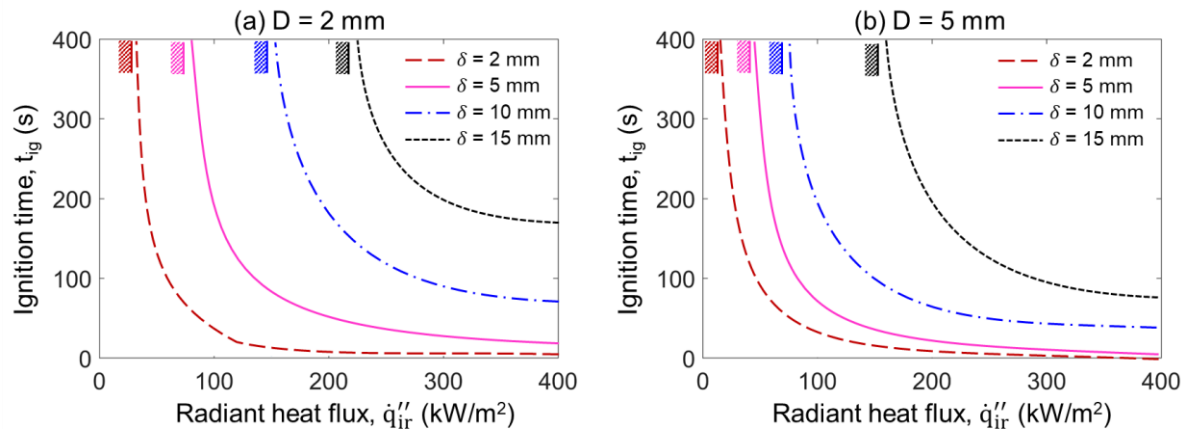

Fig. 6. Effect of sample thickness (δ) on ignition time with the irradiation spot diameter (D) of (a) 2 mm and (b) 5 mm, where the blocks represent the minimum irradiations for smoldering ignition.

For the conventional definition, a material with a thickness below 1-2 mm is often considered as thermally-thin, when it is ignited by large and uniform irradiation, the ignition time is expected to increase with the sample thickness [23]. Comparatively, for a thermally thick fuel ($\delta > 5$ mm), the ignition time is no longer sensitive to the physical thickness. Herein, we find when the sample is heated by a small irradiation spot, the ignition time continues to increase with sample thickness, even if the thickness is as large as 15 mm. Therefore, as the spot diameter decreases, the commonly used physical dimensions of thermally thin or thick fuels become inapplicable. When the irradiation spot is small, the heat conduction in the lateral direction is always significant, so the conventional assumption of the 1-D process for thermally thin and thermally thick theory is invalid. Furthermore, whether there is a critical thickness above which the ignition time is no longer sensitive to the sample thickness and how this boundary is affected by the size of the irradiation spot require further in-depth investigations.

Fig. 7 further summarizes the predicted minimum irradiation ($\dot{q}''_{min}$) of smoldering ignition vs. the sample thickness and the spot diameter. For thicker fuel samples, the minimum irradiation also decreases as the spot diameter increases, as explained by Eq. (19). On the other hand, the minimum irradiation increases with the thickness. For example, given D = 2 mm, the minimum irradiation of smoldering ignition increases from 95 kW/m^2 to 185 kW/m^2, as the thickness increases from 2 mm to 10 mm. However, as the diameter of irradiation continuously increases (D > 6 mm in Fig. 7), the sensitivity of minimum heat flux to the sample thickness decreases. From Eq. 19(b), as the diameter of the irradiation spot (D) increases, eventually, the conductive losses become negligible, and the minimum heat flux could be described as

$$\dot{q}''_{min} = \dot{q}''_{\infty,\,\text{top}} + \dot{q}''_{\infty,\,\text{bottom}} \qquad (D \gg \delta) \qquad (20)$$

which is insensitive to the sample thickness and diameter of the irradiation spot, explaining the trend in Fig. 7.

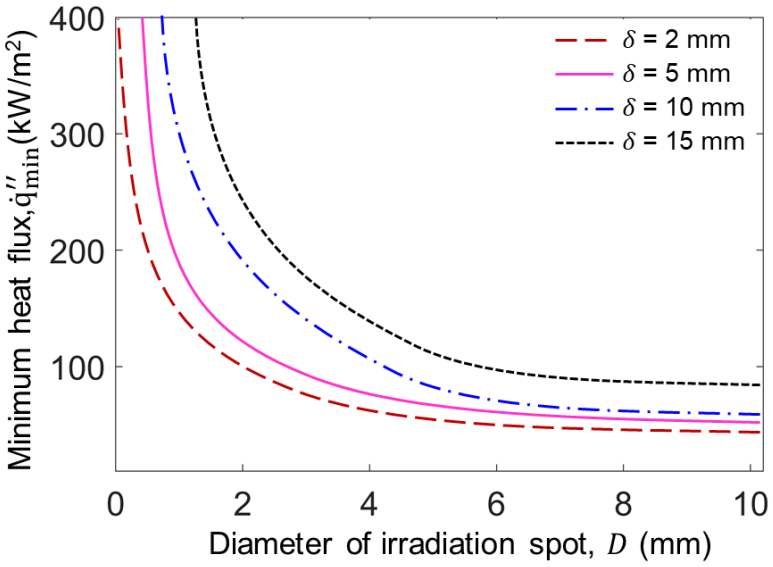

Fig. 7. Min. irradiation vs. spot diameter and fuel thickness.

3.5. Effect of fuel moisture content

Moisture may change the thermal properties of the material and enhance the heat transfer process via molecular diffusion, and it can also act as a strong heat sink during evaporation to delay the occurrence of ignition [20,57]. Therefore, it is a dominant parameter that affects the ignition process of both flaming and smoldering. Under a uniform cone irradiation, the ignition could also be delayed by the moisture content, but the ignition limits in terms of the minimum ignition temperature and irradiant level were found to be insensitive to the moisture content [20].

Herein, we further explore the effects of moisture content (dry-mass based) on the time and minimum irradiation of smoldering ignition using irradiation spots. Fig. 8(a) shows that the modeled ignition delay time increases, as the moisture content increases or the spot diameter decreases. Specifically, a 2-mm spot requires a double heating duration of the 5-mm spot and a triple heating duration of the 10-mm spot to trigger smoldering ignition.

Fig. 8(b) shows that the value of $\dot{q}''_{min}$ for spotting is insensitive to fuel moisture content, the same trend as the ignition by uniform irradiation over the entire surface (D > 60 mm) [20]. For example, given an irradiation spot of 10 mm, as the moisture content increases from 0% to 30%, the predicted minimum heat flux remains stable at 53 kW/m^2. It is because the sample will be eventually dried by long-term heating and reach the required solid-phase temperature distribution for smoldering ignition [20]. This is different from the flaming fire in the gas phase, where the water evaporated will mix with the pyrolysis gas and lower its flammability [20,23].

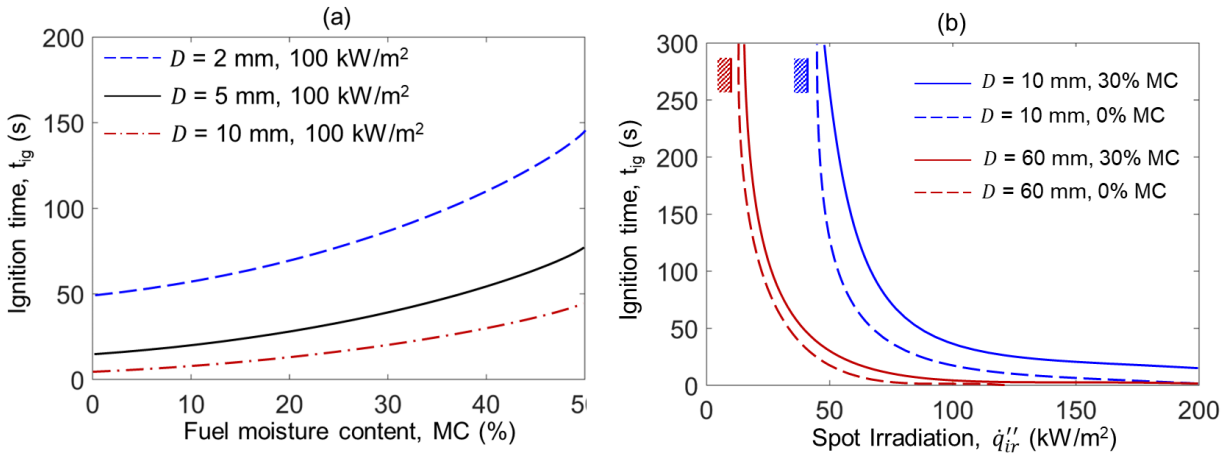

Fig. 8. Ignition delay time of smoldering spotting ignition on 2-mm thick wet fuel, (a) moisture effect, and (b) irradiation effect.

4. Conclusions

This work applies numerical simulations to investigate the smoldering ignition by an irradiation spot. The predicted ignition time decreases as the irradiation increases, following the patterns of classical piloted ignition theory. The predicted minimum irradiation of smoldering ignition increases dramatically as the diameter of irradiation spots decreases, agreeing well with the experimental

observations. A simplified heat transfer analysis is proposed to reveal the critical role of solid-phase conduction on the smoldering ignition using irradiation spots.

The constant critical ignition temperature and burning flux within the irradiated region are found to be invalid to characterize the smoldering ignition by small irradiation spots. For a thicker sample, a larger radiant heat flux and a longer heating duration are required to trigger smoldering ignition. The commonly-used physical dimension of thermally-thick fuels is not applicable because of the strong solid-phase conduction below the irradiation spot (i.e., the 1-D assumption is no longer applicable). The smoldering ignition time increases with the increasing moisture content and decreasing spot diameter. This is the first time that a comprehensive 2-D numerical model has been used to predict smoldering ignition by irradiation spot, thus helping understand the spotting fire risk in buildings and wildlands.

CRediT authorship contribution statement

Shaorun Lin: Conceptualization, Investigation, Formal analysis, Writing-original draft, Resources.
Siyan Wang: Resources.
Xinyan Huang: Conceptualization, Formal analysis, Writing-review & editing, Supervision, Funding acquisition.

Declaration of Competing Interest

The authors declare that there are no known competing financial interests or personal relationships that could have appeared to influence the work reported in this paper.

Acknowledgements

This research is funded by the National Natural Science Foundation of China (NSFC) No. 51876183 and the Joint Postdoc Scheme of The Hong Kong Polytechnic University and the University of California at Berkeley (No. P0038960).

References

[1] V. Babrauskas, Ignition Handbook, Fire Science Publishers/Society of Fire Protection Engineers, Issaquah, WA, 2003. https://doi.org/10.1023/B:FIRE.0000026981.83829.a5.

[2] S.E. Caton, R.S.P. Hakes, D.J. Gorham, A. Zhou, M.J. Gollner, Review of Pathways for Building Fire Spread in the Wildland Urban Interface Part I: Exposure Conditions, Fire Technol. 53 (2017) 429–473. https://doi.org/10.1007/s10694-016-0589-z.

[3] S.L. Manzello, S. Suzuki, M.J. Gollner, A.C. Fernandez-Pello, Role of firebrand combustion in large outdoor fire spread, Prog. Energy Combust. Sci. 76 (2020) 100801. https://doi.org/10.1016/j.pecs.2019.100801.

[4] A.C. Fernandez-Pello, Wildland fire spot ignition by sparks and firebrands, Fire Saf. J. 91 (2017) 2–10. https://doi.org/10.1016/j.firesaf.2017.04.040.

[5] J.L. Urban, C.D. Zak, J. Song, C. Fernandez-Pello, Smoldering spot ignition of natural fuels by a hot metal particle, Proc. Combust. Inst. 36 (2017) 3211–3218. https://doi.org/10.1016/j.proci.2016.09.014.

[6] S. Wang, X. Huang, H. Chen, N. Liu, G. Rein, Ignition of low-density expandable polystyrene foam by a hot particle, Combust. Flame. 162 (2015) 4112–4118. https://doi.org/10.1016/j.combustflame.2015.08.017.

[7] J.C. Jones, Thermal calculations on the ignition of a cotton bale by accidental contact with a hot particle, J. Chem. Technol. Biotechnol. 65 (1996) 176–178. https://doi.org/10.1002/(SICI)1097-4660(199602)65:2<176::AID-JCTB392>3.0.CO;2-D.

[8] J.L. Urban, C.D. Zak, C. Fernandez-Pello, Cellulose spot fire ignition by hot metal particles, Proc. Combust. Inst. 35 (2015) 2707–2714. https://doi.org/10.1016/j.proci.2014.05.081.

[9] S. Wang, X. Huang, H. Chen, N. Liu, Interaction between flaming and smouldering in hot-particle ignition of forest fuels and effects of moisture and wind, Int. J. Wildl. Fire. 26 (2017) 71–81. https://doi.org/10.1071/WF16096.

[10] R.M. Hadden, S. Scott, C. Lautenberger, C.C. Fernandez-Pello, Ignition of Combustible Fuel Beds by Hot Particles: An Experimental and Theoretical Study, Fire Technol. 47 (2011) 341–355. https://doi.org/10.1007/s10694-010-0181-x.

[11] S. Luo, Q. Xie, R. Qiu, Melting and Dripping Flow Behaviors on the Downward Flame Spread of a Wide XPS Foam, Springer US, 2019. https://doi.org/10.1007/s10694-019-00842-8.

[12] P. Sun, S. Lin, X. Huang, Ignition of thin fuel by thermoplastic drips: An experimental study for the dripping ignition theory, Fire Saf. J. 115 (2020) 103006. https://doi.org/10.1016/j.firesaf.2020.103006.

[13] S. Wang, S. Lin, Y. Liu, X. Huang, M.J. Gollner, Smoldering Ignition using a Concentrated Solar Irradiation Spot, Fire Saf. J. 129 (2022). https://doi.org/10.1016/j.firesaf.2022.103549.

[14] H. Zhang, Y. Qiao, H. Chen, N. Liu, L. Zhang, X. Xie, Experimental study on flaming ignition of pine needles by simulated lightning discharge, Fire Saf. J. (2020) 103029. https://doi.org/10.1016/j.firesaf.2020.103029.

[15] D.W. Warren, Optical Modeling of Fire Hazards Arising from Sunlight Focused by Water, Fire Technol. 50 (2014) 1327–1334. https://doi.org/10.1007/s10694-013-0353-6.

[16] R. Sun, Lincoln County fire sparked by sun rays shining through broken glass (and other unusual fire starts), The Spokesman-Review. (2018). https://www.spokesman.com/stories/2018/aug/10/summer-sparks-the-sometimes-unusual-causes-of-wild/.

[17] T.J.J. Ohlemiller, Modeling of smoldering combustion propagation, Prog. Energy Combust. Sci. 11 (1985) 277–310. https://doi.org/10.1016/0360-1285(85)90004-8.

[18] G. Rein, Smoldering combustion, in: SFPE Handb. Fire Prot. Eng., Springer, 2016: pp. 581–603.

[19] S. Lin, T.H. Chow, X. Huang, Smoldering Propagation and Blow-off on Consolidated Fuel under External Airflow, Combust. Flame. 234 (2021) 111685. https://doi.org/10.1016/j.combustflame.2021.111685.

[20] S. Lin, P. Sun, X. Huang, Can peat soil support a flaming wildfire?, Int. J. Wildl. Fire. 28 (2019) 601–613. https://doi.org/10.1071/wf19018.

[21] J. Yang, N. Liu, H. Chen, W. Gao, Smoldering and spontaneous transition to flaming over horizontal cellulosic insulation, Proc. Combust. Inst. 37 (2019) 4073–4081. https://doi.org/10.1016/j.proci.2018.05.054.

[22] B.C. Hagen, V. Frette, G. Kleppe, B.J. Arntzen, Transition from smoldering to flaming fire in short cotton samples with asymmetrical boundary conditions, Fire Saf. J. 71 (2015) 69–78. https://doi.org/10.1016/j.firesaf.2014.11.004.

[23] J.G. Quintiere, Fundamentals of Fire Phenomena, John Wiley, New York, 2006.

[24] Z. Liang, S. Lin, X. Huang, Smoldering ignition and emission dynamics of wood under low irradiation, Fire Mater. (2022) 1–11. https://doi.org/10.1002/fam.3107.

[25] R.M. Hadden, G. Rein, C.M. Belcher, Study of the competing chemical reactions in the initiation and spread of smouldering combustion in peat, Proc. Combust. Inst. 34 (2013) 2547–2553. https://doi.org/10.1016/j.proci.2012.05.060.

[26] M.T. Gratkowski, N.A. Dembsey, C.L. Beyler, Radiant smoldering ignition of plywood, Fire Saf. J. 41 (2006) 427–443. https://doi.org/10.1016/j.firesaf.2006.03.006.

[27] D.L. Simms, Experiments on the ignition on celluslosic materials by thermal radiation, Combust. Flame. 5 (1961) 369–375. https://doi.org/10.1016/0010-2180(61)90118-3.

[28] T. Kashiwagi, Experimental observation of radiative ignition mechanisms, Combust. Flame. 34 (1979) 231–244. https://doi.org/10.1016/0010-2180(79)90098-1.

[29] T. Kashiwagi, Effects of sample orientation on radiative ignition, Combust. Flame. 44 (1982) 223–245. https://doi.org/10.1016/0010-2180(82)90075-X.

[30] Y. Nakamura, T. Kashiwagi, Effects of sample orientation on nonpiloted ignition of thin poly(methyl methacrylate) sheet by a laser: 1. Theoretical prediction, Combust. Flame. 141 (2005) 149–169. https://doi.org/10.1016/j.combustflame.2004.12.014.

[31] S. Martin, Diffusion-controlled ignition of cellulosic materials by intense radiant energy, Symp. Combust. 10 (1965) 877–896. https://doi.org/10.1016/S0082-0784(65)80232-6.

[32] V. Babrauskas, Ignition of Wood : A Review of the State of the Art, J. Fire Prot. Eng. 12 (2002) 163–189. https://doi.org/10.1106/104239102028711.

[33] Y. Lizhong, Z. Yupeng, W. Yafei, D. Jiakun, D. Zhihua, Z. Xiaodong, Autoignition of solid combustibles subjected to a uniform incident heat flux: The effect of distance from the radiation source, Combust. Flame. 158 (2011) 1015–1017. https://doi.org/10.1016/j.combustflame.2011.01.008.

[34] A.M. Grishin, A.N. Golovanov, V. V. Medvedev, On the ignition of a layer of combustible forest materials by light radiation, Combust. Explos. Shock Waves. 35 (1999) 618–621. https://doi.org/10.1007/BF02674534.

[35] S. Lin, Fundamental study of near-limit smouldering fire dynamics, The Hong Kong Polytechnic University, 2021. https://theses.lib.polyu.edu.hk/handle/200/11231.

[36] F. Richter, F.X. Jervis, X. Huang, G. Rein, Effect of oxygen on the burning rate of wood, Combust. Flame. 234 (2021) 111591. https://doi.org/10.1016/j.combustflame.2021.111591.

[37] X. Huang, G. Rein, Upward-and-downward spread of smoldering peat fire, Proc. Combust. Inst. 37 (2019) 4025–4033. https://doi.org/10.1016/j.proci.2018.05.125.

[38] X. Huang, G. Rein, Downward Spread of Smoldering Peat Fire: the Role of Moisture, Density and Oxygen Supply, Int. J. Wildl. Fire. 26 (2017) 907–918. https://doi.org/10.1071/WF16198.

[39] G. Rein, a. Carlos Fernandez-Pello, D.L. Urban, Computational model of forward and opposed smoldering combustion in microgravity, Proc. Combust. Inst. 31 (2007) 2677–2684. https://doi.org/10.1016/j.proci.2006.08.047.

[40] S. Lin, H. Yuan, X. Huang, A Computational Study on the Quenching and Near-Limit Propagation of Smoldering Combustion, Combust. Flame. 238 (2022). https://doi.org/10.1016/j.combustflame.2021.111937.

[41] C. Lautenberger, Gpyro-A Generalized Pyrolysis Model for Combustible Solids: Users'Guide, Berkeley, 2016.

[42] J. Yang, H. Chen, W. Zhao, J. Zhou, TG-FTIR-MS study of pyrolysis products evolving from peat, J. Anal. Appl. Pyrolysis. 117 (2016) 296–309. https://doi.org/10.1016/j.jaap.2015.11.002.

[43] X. Huang, K. Li, H. Zhang, Modelling bench-scale fire on engineered wood : Effects of transient flame and physicochemical properties, Proc. Combust. Inst. 36 (2017) 3167–3175. https://doi.org/10.1016/j.proci.2016.06.109.

[44] K. Li, X. Huang, C. Fleischmann, G. Rein, J. Ji, Pyrolysis of Medium-Density Fiberboard : Optimized Search for Kinetics Scheme and Parameters via a Genetic Algorithm Driven by Kissinger's Method, Energy & Fuels. 28 (2014) 6130−6139. https://doi.org/10.1021/ef501380c.

[45] Y. Han, F. Richter, G. Rein, A multi-step reaction scheme to simulate self-heating ignition of coal: Effects of oxygen adsorption and smouldering combustion, Proc. Combust. Inst. 38 (2020) 4717–4725. https://doi.org/10.1016/j.proci.2020.07.016.

[46] X. Huang, G. Rein, H. Chen, Computational smoldering combustion: Predicting the roles of moisture and inert contents in peat wildfires, Proc. Combust. Inst. 35 (2015) 2673–2681. https://doi.org/10.1016/j.proci.2014.05.048.

[47] F. Richter, G. Rein, A multiscale model of wood pyrolysis in fire to study the roles of chemistry and heat transfer at the mesoscale, Combust. Flame. 216 (2020) 316–325. https://doi.org/10.1016/j.combustflame.2020.02.029.

[48] X. Huang, G. Rein, Interactions of Earth's atmospheric oxygen and fuel moisture in smouldering wildfires, Sci. Total Environ. 572 (2016) 1440–1446. https://doi.org/10.1016/j.scitotenv.2016.02.201.

[49] H. Yuan, F. Restuccia, G. Rein, Computational study on self-heating ignition and smouldering spread of coal layers in flat and wedge hot plate configurations, Combust. Flame. 214 (2020) 346–357. https://doi.org/10.1016/j.combustflame.2019.12.041.

[50] C. Lautenberger, Gpyro-A Generalized Pyrolysis Model for Combustible Solids:Technical Reference, Berkeley, 2014.

[51] H. Yuan, F. Restuccia, G. Rein, Spontaneous ignition of soils : a multi-step reaction scheme to simulate self-heating ignition of smouldering peat fires, Int. J. Wildl. Fire. (2021). https://doi.org/https://doi.org/10.1071/WF19128.

[52] X. Huang, G. Rein, Thermochemical conversion of biomass in smouldering combustion across scales: The roles of heterogeneous kinetics, oxygen and transport phenomena, Bioresour. Technol. 207 (2016) 409–421. https://doi.org/10.1016/j.biortech.2016.01.027.

[53] X. Huang, G. Rein, Smouldering combustion of peat in wildfires: Inverse modelling of the drying and the thermal and oxidative decomposition kinetics, Combust. Flame. 161 (2014) 1633–1644. https://doi.org/10.1016/j.combustflame.2013.12.013.

[54] C. Lautenberger, C. Fernandez-Pello, Generalized pyrolysis model for combustible solids, Fire Saf. J. 44 (2009) 819–839. https://doi.org/10.1016/j.firesaf.2009.03.011.

[55] F.P. Incropera, Principles of heat and mass transfer, John Wiley, 2007.

[56] S. Lin, X. Huang, J. Gao, J. Ji, Extinction of wood fire: A near-limit blue flame above smoldering surface, Fire Technol. 58 (2022) 415–434. https://doi.org/10.1007/s10694-021-01146-6.

[57] S. McAllister, Critical mass flux for flaming ignition of wet wood, Fire Saf. J. 61 (2013) 200–206. https://doi.org/10.1016/j.firesaf.2013.09.002.